J. Chem. Sci. (2021) 133:82
https://doi.org/10.1007/s12039-021-01920-7

REGULAR ARTICLE

Special Issue on Beyond Classical Chemistry

Octanuclear $\{Ln_8\}$ complexes: magneto-caloric effect in the $\{Gd_8\}$ analogue

PANKAJ KALITA[a,b], JOYDEB GOURA[a,d], PRAKASH NAYAK[a], ENRIQUE COLACIO[c,*] and VADAPALLI CHANDRASEKHAR[b,d,*]

[a]School of Chemical Sciences, National Institute of Science Education and Research, HBNI, Bhubaneswar, Jatni, Khurda 752 050, Odisha, India
[b]Centre for Interdisciplinary Sciences, Tata Institute of Fundamental Research, Gopanpally, Hyderabad 500 046, India
[c]Departamento de Química Inorgánica, Facultad de Ciencias, Universidad de Granada, Avenida de Fuentenueva s/n, 18071 Granada, Spain
[d]Department of Chemistry, Indian Institute of Technology Kanpur, Kanpur 208 016, India
E-mail: ecolacio@ugr.es; vc@tifrh.res.in; vc@iitk.ac.in

MS received 8 March 2021; revised 31 March 2021; accepted 31 March 2021

Abstract. Two neutral, isostructural, octanuclear, Ln^{III} complexes, $[Ln_8(HL)_6(L)_2(\mu_3\text{-}OH)_4(\mu_2\text{-}OH)_2(H_2O)_4]$.solv (Ln = Gd(III), ($\mathbf{1^{Gd}}$) and Dy(III), ($\mathbf{2^{Dy}}$) have been synthesized using Ln^{III} nitrate salts and a *o*-vanillin-supported multi-dentate ligand, *N'*-(2-hydroxy-3-methoxy-5-nitrobenzylidene)-2-(hydroxyamino) propanehydrazide (H_3L) in the presence of tetramethyl ammonium hydroxide. The complexes were structurally characterized by single crystal X-ray diffraction studies. The complexes are held by the cumulative coordination action of six $[HL]^{2-}$, two $[L]^{3-}$ chelating ligands, H_2O and hydroxide ligands. Magneto-structural analysis of complexes $\mathbf{1^{Gd}}$ and $\mathbf{2^{Dy}}$ reveals the presence of intramolecular antiferromagnetic interactions between the Ln^{III} ions. Magneto-caloric effect was analysed for the complex $\mathbf{1^{Gd}}$ which shows a maximum in the change of molar entropy ($-\Delta S_m$) of magnitude 25.5 J kg^{-1} K^{-1} at T = 3 K and an applied field change ΔB = 5 T.

1. Introduction

Lanthanide complexes have been of considerable research interest in recent years owing to their interesting magnetic,[1–10] optical,[11–20] and catalytic properties.[21–28] Among these systems, polynuclear complexes are formed usually as a result of the bridging ligands such as the hydroxide ligand.[29–39] Such complexes are also of interest in the field of molecular magnetism.[30,31,40–45] However, the synthesis of such complexes is fraught with some challenges. One difficulty is the formation of intractable polymeric complexes because of the ready de-protonation of the coordinated water molecules around the lanthanide ions. The formation of discrete complexes becomes feasible if controlled de-protonation of the coordinated water molecules can be achieved.[29] This is often possible by having an appropriate multi-site coordinating ligand to bind to the lanthanide ions so that the available coordination sites are reduced and the chances for the formation of a discrete complex are increased. In our lab, multi-pocket, multidentate hydrazone ligands have been extensively used for the synthesis of discrete polynuclear lanthanide complexes.[46–50] In this regard, we have designed a multi-pocket hydrazone ligand which was used to isolate dinuclear Ln^{III} complexes.[51] In these complexes, we have observed uncoordinated free oxime –OH groups which could be potentially deprotonated so that these can proliferate to form multinuclear complexes.

*For correspondence

Supplementary Information: The online version contains supplementary material available at https://doi.org/10.1007/s12039-021-01920-7.

Published online: 03 August 2021

Accordingly, herein, we report the synthesis, structures and magnetism of two octanuclear complexes, $[Ln_8(HL)_6(L)_2(\mu_3\text{–}OH)_4(\mu_2\text{–}OH)_2(H_2O)_4]$.solvents ($Ln^{III}$ = Gd^{III}, ($\mathbf{1}^{Gd}$) and Dy^{III}, ($\mathbf{2}^{Dy}$)). Interestingly, we did not use any additional co-ligand in isolating these compounds, which are often required to isolate such multinuclear Ln^{III} complexes.[52–55]

2. Experimental

2.1 *Materials and methods*

Solvents and other general reagents used in this work were obtained from commercial sources and used without further purification. 3-Methoxy-5-nitrosalicylaldehyde, hydroxylamine hydrochloride and lanthanide nitrate hydrates were obtained from Sigma Aldrich Chemical Co. (U.S.A.), Ethyl pyruvate and tetramethylammonium hydroxide pentahydrate were obtained from Spectrochem Pvt. Ltd., Mumbai, India. All these reagents were used as obtained without further purification. Ethyl (2*E*)-2-(hydroxyimino)-propanoate, (*E*)-2-(hydroxyimino)-propanehydrazide, and the ligand H_3L were prepared by a previously reported procedure.[51,56,57]

2.1a *Instrumentation*: Melting points were measured using a Stuart™ SMP10 melting point apparatus and are uncorrected. IR spectra were recorded on a Perkin Elmer FT-IR spectrometer. Mass spectra were recorded with a Bruker micrOTOF-Q II spectrometer. Elemental analyses of the compounds were obtained from a Euro Vector EA instrument (CHNS-O, model EuroEA3000).

2.1b *Magnetic measurements*: Field dependence of the magnetization at different fields and variable temperature, as well as magnetic measurements in the 2–300 K range were carried out on polycrystalline samples with a Quantum Design SQUID MPMS XL-5 device operating at different magnetic fields. Ac susceptibility measurement of $\mathbf{2}^{Dy}$ were performed using a frequency of 1400 Hz under magnetic fields of zero and 0.1 T. The static experimental susceptibilities were corrected for the diamagnetism of the constituent atoms (using Pascal's constants) and for the sample holder. To avoid any torquing of the microcrystals, a pellet of the sample cut into very small fragments were introduced in the sample holder.

2.1c *X-ray crystallography*: The molecular structures of complexes $\mathbf{1}^{Gd}$ and $\mathbf{2}^{Dy}$ were analysed by single-crystal X-ray diffraction studies performed on a Bruker APEX-II CCD diffractometer equipped with an Oxford low-temperature attachment. The crystals were kept at 120 K during data collection. The frames were indexed, integrated, and scaled using the SMART and SAINT software packages.[58] Absorption correction was performed by a multi-scan method implemented in SADABS.[59] Space groups were determined using XPREP implemented in APEX-II.[60] The structures were solved by ShelXT[61] structure solution programme using Intrinsic Phasing and refined with the ShelXL[62] refinement package using Least Squares minimization on F^2 in the Olex-2 software.[63] All the non-hydrogen atoms were refined anisotropically using full-matrix least-square procedures. Hydrogen atoms on all the bridging hydroxides were not observed in the diffraction pattern and therefore omitted entirely, although their oxidation states were confirmed by BVS calculations (see Table S1, SI).[64,65] The crystal data and the cell parameters for $\mathbf{1}^{Gd}$ and $\mathbf{2}^{Dy}$ are summarized in Table 1. The structures also contain heavily disordered solvents of crystallization which could not be modelled satisfactorily. Therefore, PLATON/SQUEEZE was used to get rid of the contributions of the disordered solvent molecules.[66] All of the mean plane analyses and molecular drawings were produced using the DIAMOND software (version 3.2).[67]

2.1d *Synthesis of metal complexes*: A general synthetic protocol was utilized for preparation of the octanuclear metal complexes as follows:

To a solution of H_3L in 20 mL of MeOH/CH_3CN (1:1 v/v), tetramethylammonium hydroxide was added. After stirring for half an hour, $Ln(NO_3)_3$·xH_2O (x = 6 for $\mathbf{1}^{Gd}$ and x = 5 for $\mathbf{2}^{Dy}$) was added to this solution which resulted in a clear yellow coloured solution. After stirring for another 12 h at room temperature the reaction mixture was filtered and kept undisturbed for crystallization. Slow evaporation of the filtrate under ambient conditions resulted in the formation of yellow block-shaped crystals suitable for X-ray diffraction after two weeks. The crystals were collected, washed with MeOH and dried under vacuum for 16 h resulting in polycrystalline powders. The specific quantities of the reactants involved in each reaction, yields of the products, and their characterization data are given below.

$[Gd_8(HL)_6(L)_2(\mu_3\text{–}OH)_4(\mu_2\text{–}OH)_2(H_2O)_4].2CH_3CN.7CH_3OH.4H_2O$ ($\mathbf{1}^{Gd}$). Quantities: H_3L (0.061 g, 0.205 mmol), $Gd(NO_3)_3$·$6H_2O$ (0.092 g, 0.205 mmol), Me_4-NOH (0.112 g, 0.616 mmol). Yield: 0.066 g (49%

Table 1. Crystallographic details for complexes $\mathbf{1^{Gd}}$ and $\mathbf{2^{Dy}}$.

	$\mathbf{1^{Gd}}$	$\mathbf{2^{Dy}}$
Empirical formula*	$C_{88}H_{86}Gd_8N_{32}O_{58}$	$C_{88}H_{86}Dy_8N_{32}O_{58}$
Formula weight*	3777.88	3819.88
Temperature/K	120(2)	120(0)
Crystal system	Monoclinic	Monoclinic
Space group	*C*2/c	*C*2/c
a/Å	19.1263(18)	18.9896(19)
b/Å	31.7579(18)	31.583(3)
c/Å	25.4695(16)	25.239(3)
α/°	90	90
β/°	98.198(5)	98.325(5)
γ/°	90	90
Volume/Å^3	15312.4(19)	14978(3)
Z	4	4
ρ^{calc} g/cm^3	1.639	1.694
μ/mm^{-1}	3.500	4.027
F(000)	7256.0	7320.0
Crystal size/mm^3	0.21 × 0.15 × 0.11	0.13 × 0.11 × 0.08
Radiation	MoKα (λ = 0.71073)	MoKα (λ = 0.71073)
2θ range for data collection/°	2.504 to 51.332	3.052 to 57.938
Index ranges	− 22 ≤ h ≤ 23, − 38 ≤ k ≤ 38, − 30 ≤ l ≤ 24	− 25 ≤ h ≤ 25, − 42 ≤ k ≤ 41, − 30 ≤ l ≤ 33
Reflections collected	85743	114164
Independent reflections	14325 [R_{int} = 0.1923]	18900 [R_{int} = 0.2075]
Data/restraints/parameters	14325/1/630	18900/2/797
GOF on F^2	1.029	0.948
Final R indexes [I >= 2σ (I)]	R_1 = 0.1065, wR_2 = 0.2123	R_1 = 0.0660, wR_2 = 0.1317
Final R indexes [all data]	R_1 = 0.2235, wR_2 = 0.2758	R_1 = 0.1692, wR_2 = 0.1690
CCDC Number	2064754	2064755

*including H atoms of the bridging hydroxyl groups as confirmed by BVS calculations.

based on Gd). M.p.: >250 °C. IR (KBr) (cm^{-1}): 3425(br), 3245(w), 2941(w), 2839(w), 1605(s), 1570(m), 1493(s), 1383(s), 1360(w), 1305(s), 1256(m), 1203(m), 1101(s), 1060 (m), 975(w), 911(s), 842(w), 777(m), 746(m), 725(w), 707(w), 552(w). Calcd. for $C_{88}H_{86}Gd_8N_{32}O_{58}$ (MW = 3777.82): C, 28.61; H, 3.10; N, 11.46. Found: C, 28.42; H, 2.89; N, 11.17 ESI-MS: m/z = 1868.9176, $[Gd_8(HL)_6(L)_2(OH)_6 + Na^+ + H^+]^{2+}$.

$[Dy_8(HL)_6(L)_2(\mu_3\text{–}OH)_4(\mu_2\text{–}OH)_2(H_2O)_4].CH_3CN.5CH_3OH.9H_2O$ ($\mathbf{2^{Dy}}$). H_3L (0.061 g, 0.205 mmol), $Dy(NO_3)_3{\cdot}5H_2O$ (0.090 g, 0.205 mmol), Me_4NOH (0.111 g, 0.616 mmol). Yield: 0.066 g (49% based on Dy). M.p.: >250 °C. IR (KBr) (cm^{-1}): 3417(br), 3235(w), 2939(w), 2837(w), 1603(s), 1568(m), 1491(s), 1381(s), 1360(w), 1306(s), 1254(m), 1201(m), 1101(s), 1058(m), 975(w), 909(s), 842(w), 777(m), 746(m), 726(w), 705(w), 552(w). Calcd for $C_{88}H_{86}Dy_8N_{32}O_{58}$ (MW = 3819.82): C, 27.28; H, 3.06; N, 11.05. Found: C, 27.06; H, 2.81; N, 10.77. ESI-MS: m/z = 1889.9365, $[Dy_8(HL)_6(L)_2(OH)_6 + Na^+ + H^+]^{2+}$.

3. Results and Discussion

3.1 *Synthetic aspects*

The Schiff base hydrazone ligand, *N*'-(2-hydroxy-3-methoxy-5-nitrobenzylidene)-2-(hydroxyamino)propanehydrazide (H_3L), contains six potential coordinating sites capable of binding to multiple lanthanide metal ions in different coordination modes as shown in Scheme 1. The role of the hydroxide base is crucial not only in deprotonating H_3L but also for being a source of hydroxide ligands essential for stitching the multiple metal centres together in the complexes without the need for additional co-ligands. Thus, the reaction of H_3L with hydrated $Ln(NO_3)_3{\cdot}xH_2O$ and $Me_4NOH.5H_2O$ in the 1:1:3 molar ratio in

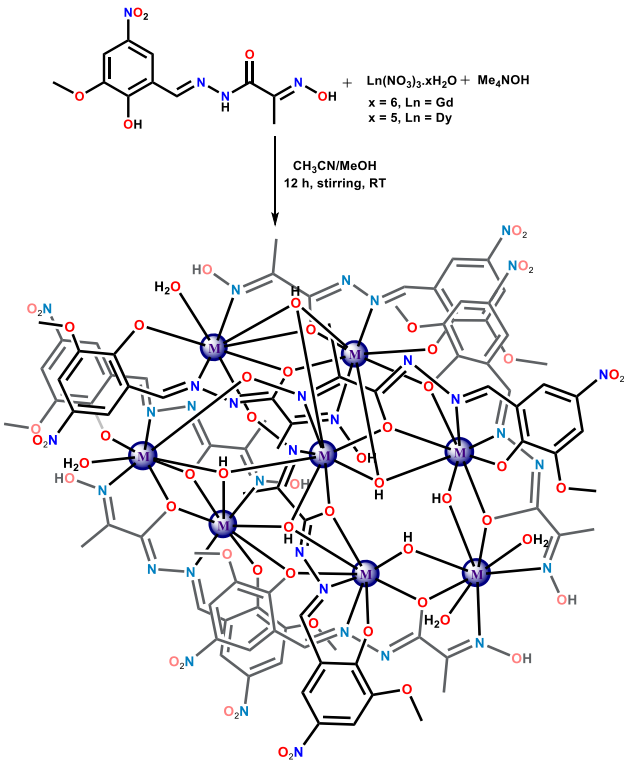

Scheme 1. Synthesis of complexes $\mathbf{1}^{\mathbf{Gd}}$ and $\mathbf{2}^{\mathbf{Dy}}$.

MeOH/CH_3CN (v/v) solvent mixture allowed isolation of $[Ln_8(HL)_6(L)_2(\mu_3\text{–}OH)_4(\mu_2\text{–}OH)_2(H_2O)_4]$ complexes (Scheme 1).

ESI-MS studies of $\mathbf{1}^{\mathbf{Gd}}$ and $\mathbf{2}^{\mathbf{Dy}}$ revealed that all the complexes retain their molecular ion peaks at m/z = 1868.9176 and 1889.9365 corresponding to the dicationic fragments $[Gd_8(HL)_6(L)_2(OH)_6 + Na^+ + H^+]^{2+}$ and $[Dy_8(HL)_6(L)_2(OH)_6 + Na^+ + H^+]^{2+}$. The ESI-MS of $\mathbf{2}^{\mathbf{Dy}}$ is shown in Figure 1 while that of $\mathbf{1}^{\mathbf{Gd}}$ is shown in Figure S1, SI.

3.2 *Molecular structures*

The molecular structures of the complexes $\mathbf{1}^{\mathbf{Gd}}$ and $\mathbf{2}^{\mathbf{Dy}}$ were confirmed by the single crystal X-ray studies. Both the complexes are charge neutral and crystallized in the monoclinic crystal system in the *C*2c space group (Z = 4). The octanuclear complexes comprise of eight Ln^{III} cations, six $[HL]^{2-}$, two $[L]^{3-}$, four $[\mu_3\text{–}OH]^-$, two $[\mu_2\text{–}OH]^-$ anions, and four H_2O molecules (Figure 2). Considering the overall structural similarity of these two complexes, we have chosen $\mathbf{1}^{\mathbf{Gd}}$ to elucidate the common structural features present in them. The molecular structure of $\mathbf{2}^{\mathbf{Dy}}$ is shown in Figure S2 (SI) and the corresponding interatomic distance parameters are given in Table S5 (SI).

The molecular structure of $\mathbf{1}^{\mathbf{Gd}}$ and its asymmetric unit are given in Figure 2. A C_2 axis passes through the line connecting the Gd1 and Gd5 which equally divides the whole molecule into two halves generating the asymmetric unit. The formation of the octanuclear complex can be understood as follows. The whole molecular structure can be viewed as being composed of (*i*) a tetranuclear core (Figure 3(a)) and (*ii*) two structurally similar dinuclear motifs (Figure 3(b)). In the dinuclear cores, the two $[HL]^{2-}$ ligands hold two Gd^{III} ions in a 'head-to-tail' fashion utilizing a tridentate (O, N, O) and a bidentate (N, O) coordinating motif. The enolate oxygen atoms (O2 and O2*) of the ligand bridge the two metal centres affording an approximate rhomboidal-shaped four-membered Gd_2O_2 core. The average Gd···Gd distance and average Gd−O_{enol}−Gd angle in the Gd_2O_2 cores are found to be 3.677(19) Å and 103.365(62)°, respectively. Each of the Gd^{III} ions in the dinuclear units is eight-coordinate with an overall 2N, 6O coordination environment. In the tetranuclear unit, one $[HL]^{2-}$ ligand and one $[L]^{3-}$ ligand hold three Gd^{III} ions in a 'head-to-head' fashion. The bridging coordination action of the enolate oxygen atoms and the hydroxyl atoms between the four metal centres results in a Gd_4O_8 core where the four metal ions are present in a *kite*-shaped geometry. The average Gd···Gd distance and the average Gd−O_{enol}−Gd angle in this core are found to be 3.831(18) Å and 107.071(59)°, respectively. The overall coordination environment around the metal ions in this core is also 2N, 6O similar to the coordination environment observed in the dinuclear units. The cumulative coordination action of the hydroxyl anions and the ligand oxime oxygen atoms connects the two dinuclear units with the tetranuclear unit completing the octanuclear {Gd_8} complex. Selected interatomic distances and bond angle parameters of $\mathbf{1}^{\mathbf{Gd}}$ are given in Table S2 (SI).

A view of the {Gd_8} core with only the bridging atoms is shown in Figure 4 (*left*). Mean plane analysis reveals that the *kite*-shaped {Gd_4} unit is perfectly planar comprising the Gd1, Gd2, Gd2*, and Gd5 atoms (*plane 1*). Another two planes corresponding to the dinuclear units i.e., *plane 2* (Gd1, Gd3, Gd4) and *plane 3* (Gd1, Gd3*, Gd4*) are at a dihedral angle of 62.97(3)° with respect to *plane* 1 while the *plane 2* and *plane 3* bisects one another with a dihedral angle of 33.57(5)° (Figure 4 (*right*))

The immediate coordination geometries around all the eight Gd atoms were confirmed by the SHAPE analysis.[68,69] The geometries were obtained as square antiprism (Gd1, Gd2, Gd2*), Johnson gyrobifastigium (Gd3, Gd3*), biaugmented trigonal prism (Gd4,

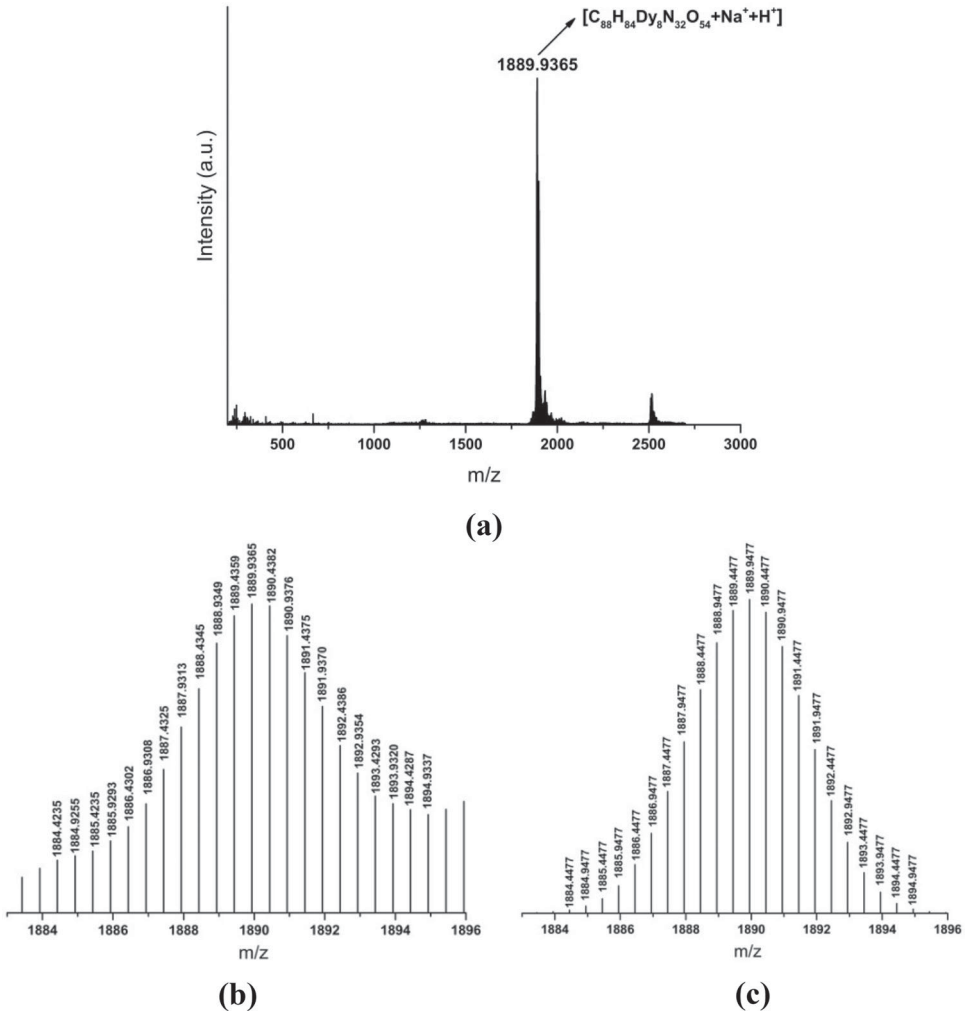

Figure 1. (**a**) Full range ESI-MS spectrum of complex $\mathbf{2}^{\mathbf{Dy}}$. (**b**) Experimental and (**c**) Simulated pattern of $[Dy_8(HL)_6(L)_2(OH)_6 + Na^+ + H^+]^{2+}$.

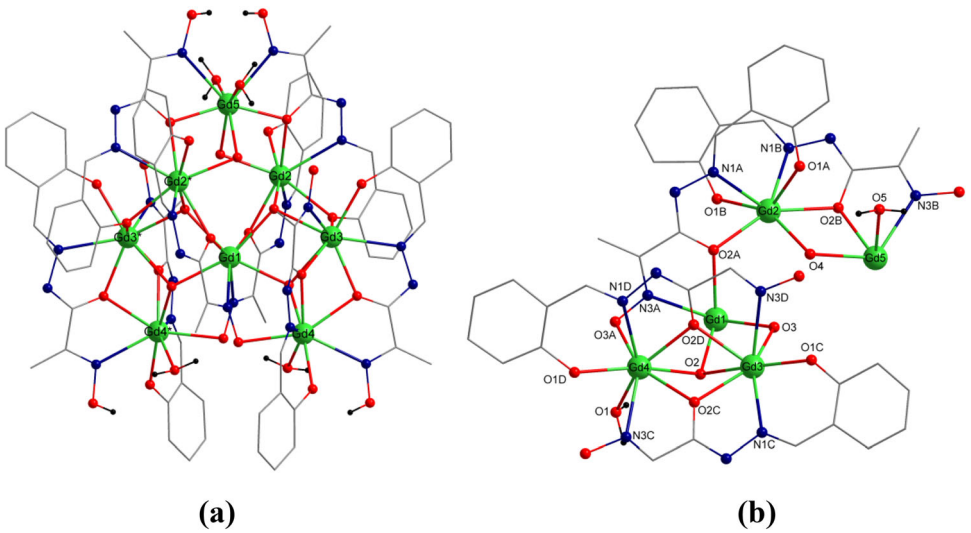

Figure 2. (**a**) The molecular structure of $\mathbf{1}^{\mathbf{Gd}}$ (–OMe, $–NO_2$ groups, and H atoms except in the water molecules are omitted for clarity) and (**b**) the asymmetric unit of the complex Colour scheme: Gd^{III}, light green; O, red; N, blue; C, gray.

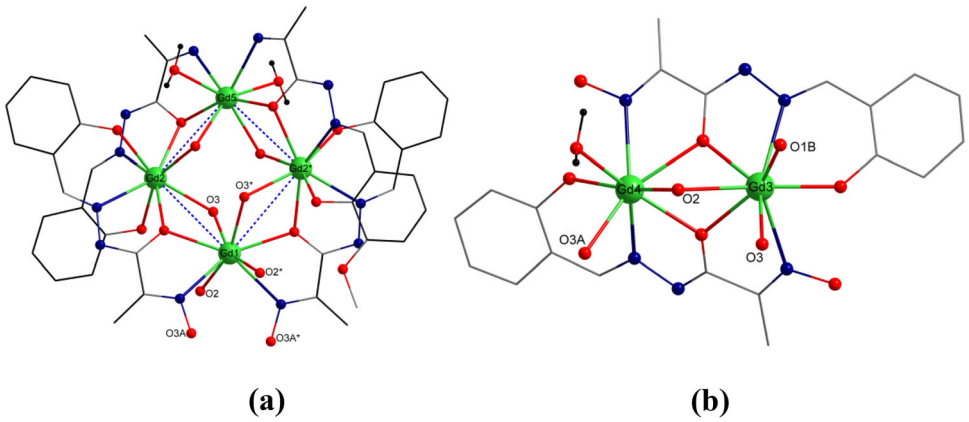

Figure 3. (**a**) The tetranuclear core and (**b**) the dinuclear core of $\mathbf{1}^{\mathbf{Gd}}$.

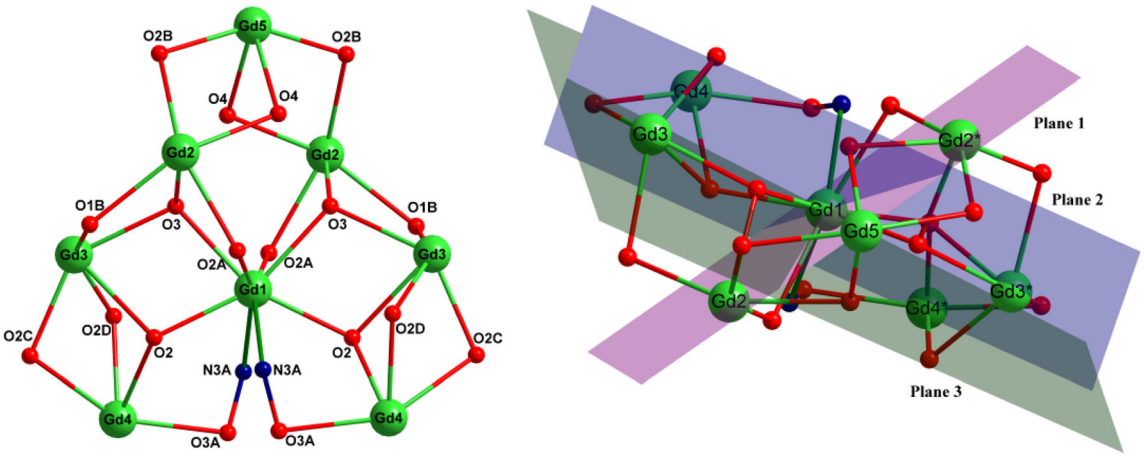

Figure 4. (*left*) The structure of the $\{Gd_8\}$ core motif and (*right*) the mean planes in the structure of complex $\mathbf{1}^{\mathbf{Gd}}$.

Gd4*), and triangular dodecahedron (Gd5) (Figure S3 and Tables S3 and S4, SI). Similar types of coordination environments were also observed in the complex $\mathbf{2}^{\mathbf{Dy}}$. The packing diagram (Figure S5, SI) shows that the shortest Gd···Gd separation between two adjacent $\{Gd_8\}$ molecules is 9.215 Å.

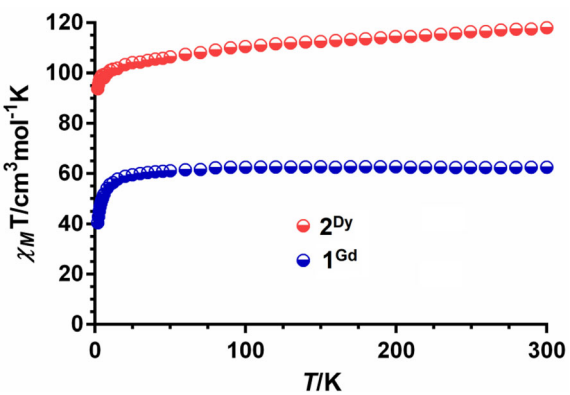

Figure 5. Temperature dependence of the $\chi_M T$ product for complexes $\mathbf{1}^{\mathbf{Gd}}$ and $\mathbf{2}^{\mathbf{Dy}}$.

3.3 *Magnetic properties*

The temperature dependence of $\chi_M T$ for complexes $\mathbf{1}^{\mathbf{Gd}}$ and $\mathbf{2}^{\mathbf{Dy}}$ (χ_M is the molar magnetic susceptibility per Ln_8 unit) in the range 2-300 K were measured under a magnetic field of 0.1 T (Figure 5).

The $\chi_M T$ product for $\mathbf{1}^{\mathbf{Gd}}$ at room temperature (62.60 cm^3 K mol^{-1}) agrees well with that expected for eight isolated Gd^{III} ions with g = 2 and S = 7/2 (63 cm^3 K mol^{-1} for g = 2). By lowering the temperature, the $\chi_M T$ product remains almost constant until ~ 100 K and then decreases sharply down to 2 K to reach a value of (39.40 cm^3 K mol^{-1}). The decrease of the χT product at low temperature is mainly due to an overall weak antiferromagnetic interaction between the Gd^{III} ions, combined with very small ZFS of the

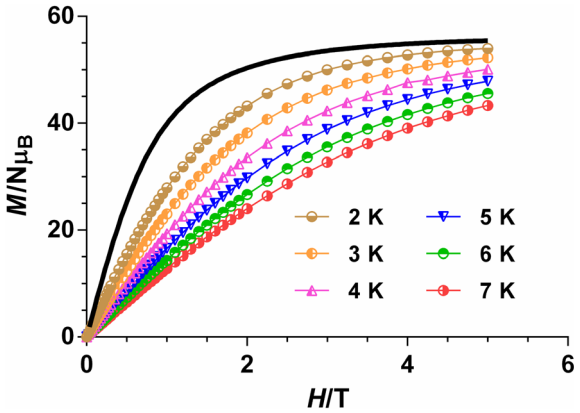

Figure 6. The field dependence of the magnetization plots for $\mathbf{1}^{\mathbf{Gd}}$ between 2 and 7 K. The black solid line corresponds to the Brillouin function for eight uncoupled Gd^{III} ions.

ground state (the Gd^{III} ion is an essentially isotropic ion) and Zeeman effects. The magnitude of the antiferromagnetic exchange interaction in $\mathbf{1}^{\mathbf{Gd}}$ could not be determined by diagonalization matrix methods because of the extremely high dimension of the matrices to be diagonalized for a Gd_8 system.

The existence of antiferromagnetic interactions between the Gd^{III} ions is supported by the field dependence of the magnetization at 2 K which is well below the Brillouin function for eight non-interacting Gd^{III} ions (Figure 6). At high field, the saturation of the magnetization is almost complete at 5 T (54 μ_B), reaching values that agree well with the theoretical saturation values for eight Gd^{III} ions (56 μ_B).

Experimental and theoretical studies[70–72] carried out on oxygen-bridged Gd_2 complexes (alkoxido, phenoxido and carboxylate) have suggested that J becomes more antiferromagnetic as the Gd–O–Gd angle (θ), and consequently the Gd···Gd distance, decrease, and the Gd–O distances become more equal. The crossing point between antiferromagnetic and ferromagnetic interactions occurs approximately at θ and Gd···Gd values of 112° and 4.0 Å, respectively. The global antiferromagnetic interaction observed in complex $\mathbf{1}^{\mathbf{Gd}}$ is not unexpected because, except for one angle (117.39°) and one distance (4.076 Å), in the asymmetric unit all the θ angles (in the 3.677–3.887 Å range) and Gd···Gd distances (in the 96.70–109.02°) are below the above values.

It is worth mentioning that low temperature molecular magnetic coolers (MMCs) based on Gd^{III} complexes can exhibit higher magneto-caloric effects (MCEs), that is to say, an important change of magnetic entropy upon application of a magnetic field.[73] This effect is of great interest because Gd^{III} complexes with high MCE could be potentially employed for refrigeration applications *via* adiabatic demagnetization.[73] We have studied the MCE properties of $\mathbf{1}^{\mathbf{Gd}}$ because of the following reasons. (*i*) The Gd^{III} ion exhibits negligible anisotropy due to the absence of orbital contribution and the largest single-ion spin ($S = 7/2$) arising from the $4f^7$ electron configuration. Both factors (small anisotropy and large spin ground state) favour an enhanced MCE. (*ii*) The weak antiferromagnetic interactions between the Gd^{III} ions give rise to multiple low-lying excited and field-accessible spin states, very close in energy with respect to each other, each of which can contribute to the magnetic entropy of the system.

In view of the above considerations, a significant magneto-caloric effect is expected for $\mathbf{1}^{\mathbf{Gd}}$. The magnetic entropy changes ($-\Delta S_m$) that characterize the magneto-caloric properties of $\mathbf{1}^{\mathbf{Gd}}$ were calculated from the experimental isothermal field dependent magnetization data (Figure 7) by making use of the Maxwell relation:

$$\Delta S_M = (T, \Delta B) = \int_{B_i}^{B_f} \left[\frac{\partial M(T,B)}{dT}\right]_B dB$$

where B_i and B_f are the initial and final applied magnetic fields. The values of $-\Delta S_m$ for $\mathbf{1}^{\mathbf{Gd}}$ (Figure 7) under all magnetic fields increase with decreasing temperature from 7 to 3 K. The maximum value of $-\Delta S_m$ achieved for $\mathbf{1}^{\mathbf{Gd}}$ is 25.5 J kg^{-1} K^{-1} at $T = 3$ K and applied field change $\Delta B = 5$ T (Figure 6). Despite the antiferromagnetic interactions between the Gd^{III} ions in $\mathbf{1}^{\mathbf{Gd}}$, there is an important change in $-\Delta S_m$, which is due to the easy spin polarization at a relatively low magnetic field. The extracted $-\Delta S_m$ value at $T = 3$ K is lower than that calculated for the full magnetic entropy content per mole $nR\ln(2S_{Gd} + 1) = 16.6$ R = 35.1 J kg^{-1} K^{-1}. This is essentially due to the existence of

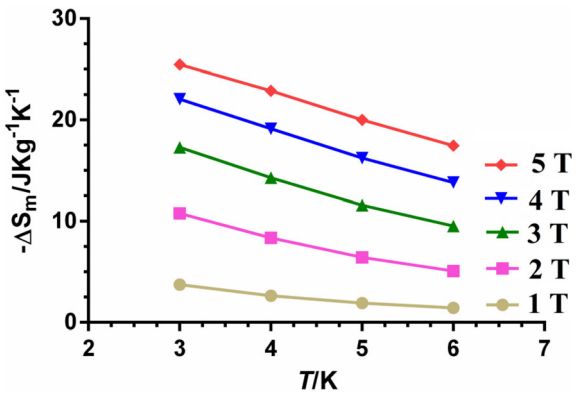

Figure 7. The magnetic entropy changes ($-\Delta S_m$) calculated using the magnetization data for $\mathbf{1}^{\mathbf{Gd}}$ from 1 to 5 T and temperatures from 3 to 7 K.

antiferromagnetic interactions between the Gd^{III} ions. It should be noted that the extracted $-\Delta S_m$ value at 5 T for $\mathbf{1^{Gd}}$ is close to that found for alkoxido/hydroxo bridged Gd_8 complexes with antiferromagnetic interaction between the Gd^{III} ions and possessing similar molecular weight (M_w),[74–76] but lower than that found for other much more magnetically dense Gd^{III} complexes (M_w/N, where N = number of Gd^{3+} ions).[77–83]

It is well known that Dy^{III} complexes are good candidates to exhibit slow relaxation of the magnetization because Dy^{III} is a Kramers ion with a bistable ground state (electronic structure composed of Kramers doublets, KDs) and a large magnetic moment. In addition to this, to observe slow magnetization relaxation, the ground state must be axial, to possess the largest value of M_J ($\pm$ 15/2). This KD can be stabilized by an axial crystal field because the repulsive interactions between the ligands and its disc shape charge cloud are minimized.[84] It is worth noting that the axial ligand field can be attained by serendipity in low symmetry Dy^{III} complexes and, therefore, they often exhibit slow relaxation of the magnetization and SMM behaviour.

In view of the above considerations, we have performed ac magnetic susceptibility measurements under zero- and small-applied *dc* magnetic fields to know if $\mathbf{2^{Dy}}$ exhibits slow relaxation of the magnetization. The results of these measurements demonstrate that compound $\mathbf{2^{Dy}}$ does not exhibit any maximum above 2 K in the out-of-phase (χ“$_M$) signals even at the highest used frequency of 1400 Hz (Figure S6, SI). This behaviour could be due to a fast relaxation of the magnetization through quantum tunneling (QTM) and/or to the existence of a very small effective energy barrier that is not able to trap the magnetization in one of the two equivalent orientations at temperatures above 2 K. When the ac measurements were carried out in the presence of a small external dc field of 1000 Oe (Figure S6, SI), to fully or partly suppress the possible fast quantum tunneling relaxation, the temperature dependence of χ''_M for $\mathbf{2^{Dy}}$ at 1400 Hz did not significantly change. This either supports a very small height of anisotropic energy barrier (typically below 5 K) or suggests that the strong QTM process, leading to apparently lower U_{eff} values, is not effectively suppressed by the field and therefore should have its origin in hyperfine and intramolecular/intermolecular magnetic interactions.

4. Conclusions

In conclusion, we have demonstrated a *cluster expansion* synthetic method to assemble discrete multinuclear Ln^{III} complexes [Ln^{III} = Gd^{III}/Dy^{III}]. The structural topology of these complexes is quite unprecedented among the known {Ln_8} topologies. The two complexes are also quite stable in the solution phase as confirmed by their ESI-MS studies. We have studied the magnetic properties of the Gd^{III} and Dy^{III} derivatives. Although the Dy^{III} derivative shows a slow magnetic relaxation at very low temperature and at a high frequency in the ac susceptibility measurements a clear maxima was not observed. The Gd^{III} derivative being isotropic and the Gd^{III} ions interacting in a weakly antiferromagnetic manner, the magnetocaloric effect in this complex was studied from the magnetization vs field data at different temperatures. This study reveals a maximum in the change of molar entropy ($-\Delta S_m$) of magnitude 25.5 J kg^{-1} K^{-1} at T = 3 K and an applied field change ΔB = 5 T.

Supplementary Information (SI)

Scheme S1, Tables S1-S5, Figures S1-S6 are available at www.ias.ac.in/chemsci.

References

1. Woodruff D N, Winpenny R E P and Layfield R A 2013 Lanthanide single-molecule magnets *Chem. Rev.* **113** 5110
2. Bar A K, Kalita P, Singh M K, Rajaraman G and Chandrasekhar V 2018 Low-coordinate mononuclear lanthanide complexes as molecular nanomagnets *Coord. Chem. Rev.* **367** 163
3. Ding Y-S, Chilton N F, Winpenny R E P and Zheng Y-Z 2016 On approaching the limit of molecular magnetic anisotropy: a near-perfect pentagonal bipyramidal dysprosium(III) single-molecule magnet *Angew Chem. Int. Ed.* **55** 16071
4. Pointillart F, Cador O, Le Guennic B and Ouahab L 2017 Uncommon lanthanide ions in purely 4f single molecule magnets *Coord. Chem. Rev.* **346** 150
5. Gould C A, Darago L E, Gonzalez M I, Demir S and Long J R 2017 A trinuclear radical-bridged lanthanide single-molecule magnet *Angew. Chem. Int. Ed.* **56** 10103
6. Goodwin C A P, Ortu F, Reta D, Chilton N F and Mills D P 2017 Molecular magnetic hysteresis at 60 kelvin in dysprosocenium *Nature* **548** 439
7. Latendresse T P, Bhuvanesh N S and Nippe M 2017 Slow magnetic relaxation in a lanthanide-[1]metallocenophane complex *J. Am. Chem. Soc.* **139** 8058
8. Guo F-S, Day B M, Chen Y-C, Tong M-L, Mansikkamäki A and Layfield R A 2018 Magnetic hysteresis up to 80 kelvin in a dysprosium metallocene single-molecule magnet *Science* **362** 1400
9. Harriman K L M, Brosmer J L, Ungur L, Diaconescu P L and Murugesu M 2017 Pursuit of record breaking energy barriers: a study of magnetic axiality in diamide

ligated DyIII single-molecule magnets *J. Am. Chem. Soc.* **139** 1420
10. Pedersen K S, Ariciu A-M, McAdams S, Weihe H, Bendix J, Tuna F and Piligkos S 2016 Toward molecular 4f single-ion magnet qubits *J. Am. Chem. Soc.* **138** 5801
11. Ning Y, Cheng S, Wang J-X, Liu Y-W, Feng W, Li F and Zhang J-L 2019 Fluorescence lifetime imaging of upper gastrointestinal pH in vivo with a lanthanide based near-infrared τ probe *Chem. Sci.* **10** 4227
12. Bünzli J-CG 2016 Lanthanide light for biology and medical diagnosis *J. Lumin.* **170** 866
13. Carlos L D, Ferreira R A S, de Zea Bermudez V, Julián-López B and Escribano P 2011 Progress on lanthanide-based organic–inorganic hybrid phosphors *Chem. Soc. Rev.* **40** 536
14. Chen P, Li Q, Grindy S and Holten-Andersen N 2015 White-light-emitting lanthanide metallogels with tunable luminescence and reversible stimuli-responsive properties *J. Am. Chem. Soc.* **137** 11590
15. Cho U, Riordan D P, Ciepla P, Kocherlakota K S, Chen J K and Harbury P B 2017 Ultrasensitive optical imaging with lanthanide lumiphores *Nat. Chem. Biol.* **14** 15
16. Wartenberg N, Raccurt O, Bourgeat-Lami E, Imbert D and Mazzanti M 2013 Multicolour optical coding from a series of luminescent lanthanide complexes with a unique antenna *Chem. Eur. J.* **19** 3477
17. Xu L-J, Xu G-T and Chen Z-N 2014 Recent advances in lanthanide luminescence with metal-organic chromophores as sensitizers *Coord. Chem. Rev.* **273–274** 47
18. Xu Y-Y, Chen P, Gao T, Li H-F and Yan P-F 2019 White-light emission based on a single component Sm(III) complex and enhanced optical properties by doping methods *CrystEngComm* **21** 964
19. Yang X, Lin X, Zhao Y, Zhao Y S and Yan D 2017 Lanthanide metal-organic framework microrods: colored optical waveguides and chiral polarized emission *Angew. Chem. Int. Ed.* **56** 7853
20. Zhou Y, Zhang H-Y, Zhang Z-Y and Liu Y 2017 Tunable luminescent lanthanide supramolecular assembly based on photoreaction of anthracene *J. Am. Chem. Soc.* **139** 7168
21. Jenks T C, Bailey M D, Hovey Jessica L, Fernando S, Basnayake G, Cross M E, et al. 2018 First use of a divalent lanthanide for visible-light-promoted photoredox catalysis *Chem. Sci.* **9** 1273
22. Qin J, Xu B, Zhang Y, Yuan D and Yao Y 2016 Cooperative rare earth metal–zinc based heterometallic catalysts for copolymerization of CO_2 and cyclohexene oxide *Green Chem.* **18** 4270
23. Kazeminejad N, Munzel D, Gamer M T and Roesky P W 2017 Bis(amidinate) ligands in early lanthanide chemistry-synthesis, structures, and hydroamination catalysis *Chem Commun.* **53** 1060
24. Dochain S, Vetica F, Puttreddy R, Rissanen K and Enders D 2016 Combining organocatalysis and lanthanide catalysis: a sequential one-pot quadruple reaction sequence/hetero-diels–alder asymmetric synthesis of functionalized tricycles *Angew. Chem. Int. Ed.* **128** 16387
25. Nagae H, Aoki R, Akutagawa S-n, Kleemann J, Tagawa R, Schindler T, et al. 2018 Lanthanide complexes supported by a trizinc crown ether as catalysts for alternating copolymerization of epoxide and CO_2: telomerization controlled by carboxylate anions *Angew. Chem. Int. Ed.* **57** 2492
26. Han Q, Wang L, Shi Z, Xu C, Dong Z, Mou Z and Liu W 2017 Self-assembly of luminescent lanthanide mesocates as efficient catalysts for transforming carbon dioxide into cyclic carbonates *Chem. Asian J.* **12** 1364
27. Halter D P, Palumbo C T, Ziller J W, Gembicky M, Rheingold A L, Evans W J and Meyer K 2018 Electrocatalytic H_2O reduction with f-elements: mechanistic insight and overpotential tuning in a series of lanthanide complexes *J. Am. Chem. Soc.* **140** 2587
28. Pagis C, Ferbinteanu M, Rothenberg G and Tanase S 2016 Lanthanide-based metal organic frameworks: synthetic strategies and catalytic applications *ACS Catal.* **6** 6063
29. Zhang Z, Zhang Y and Zheng Z 2016 In *Recent Development in Clusters of Rare Earths and Actinides: Chemistry and Materials* Z Zheng (Ed.) (Berlin, Heidelberg: Springer) Vol. 173
30. Le Natur F, Calvez G, Guégan J-P, Le Pollès L, Trivelli X, Bernot K, et al. 2015 Characterization and luminescence properties of lanthanide-based polynuclear complexes nanoaggregates *Inorg. Chem.* **54** 6043
31. Zhou Y, Zheng X-Y, Cai J, Hong Z-F, Yan Z-H, Kong X-J, et al. 2017 Three giant lanthanide clusters Ln_{37} (Ln = Gd, Tb, and Eu) featuring A double-cage structure *Inorg. Chem.* **56** 2037
32. Luo T-Y, Liu C, Eliseeva S V, Muldoon P F, Petoud S and Rosi N L 2017 Rare earth pcu metal-organic framework platform based on $RE_4(\mu_3\text{-}OH)_4(COO)_6^{2+}$ clusters: rational design, directed synthesis, and deliberate tuning of excitation wavelengths *J. Am. Chem. Soc.* **139** 9333
33. Guo F-S, Chen Y-C, Mao L-L, Lin W-Q, Leng J-D, Tarasenko R, et al. 2013 Anion-TEMPlated assembly and magnetocaloric properties of a nanoscale Gd38 cage versus a Gd48 barrel *Chem. Eur. J.* **19** 14876
34. Thielemann D T, Wagner A T, Lan Y, Oña-Burgos P, Fernández I, Rösch E S, et al. 2015 Peptoid-ligated pentadecanuclear yttrium and dysprosium hydroxy clusters *Chem. Eur. J.* **21** 2813
35. Wang W-M, Wu Z-L, Zhang Y-X, Wei H-Y, Gao H-L and Cui J-Z 2018 Self-assembly of tetra-nuclear lanthanide clusters via atmospheric CO_2 fixation: interesting solvent-induced structures and magnetic relaxation conversions *Inorg. Chem. Front.* **5** 2346
36. Zheng X-Y, Peng J-B, Kong X-J, Long L-S and Zheng L-S 2016 Mixed-anion templated cage-like lanthanide clusters: Gd_{27} and Dy_{27} *Inorg. Chem. Front.* **3** 320
37. Calvez G, Le Natur F, Daiguebonne C, Bernot K, Suffren Y and Guillou O 2017 Lanthanide-based hexanuclear complexes and their use as molecular precursors *Coord.Chem. Rev.* **340** 134
38. Omagari S, Nakanishi T, Kitagawa Y, Seki T, Fushimi K, Ito H, et al. 2016 Critical role of energy transfer between terbium ions for suppression of back energy transfer in nonanuclear terbium clusters *Sci. Rep.* **6** 37008

39. Zheng X-Y, Xie J, Kong X-J, Long L-S and Zheng L-S 2019 Recent advances in the assembly of high-nuclearity lanthanide clusters *Coord. Chem. Rev.* **378** 222
40. Xiong J, Ding H-Y, Meng Y-S, Gao C, Zhang X-J, Meng Z-S, et al. 2017 Hydroxide-bridged five-coordinate DyIII single-molecule magnet exhibiting the record thermal relaxation barrier of magnetization among lanthanide-only dimers *Chem. Sci.* **8** 1288
41. Qin L, Yu Y-Z, Liao P-Q, Xue W, Zheng Z, Chen X-M and Zheng Y-Z 2016 A "molecular water pipe": a giant tubular cluster Dy72 exhibits fast proton transport and slow magnetic relaxation *Adv. Mater.* **28** 10772
42. Wang G, Wei Y and Wu K 2016 Goblet-shaped pentanuclear lanthanide clusters assembled with a cyclen derivative ligand exhibiting slow magnetic relaxation *Dalton Trans.* **45** 12734
43. Ibrahim M, Mereacre V, Leblanc N, Wernsdorfer W, Anson C E and Powell A K 2015 Self-assembly of a giant tetrahedral 3 d–4 f Single-molecule magnet within a polyoxometalate system *Angew. Chem. Int. Ed.* **54** 15574
44. An R, Chen X-L, Hu H-M, Ren Y-L, Wu Q-R and Xue G-L 2015 Synthesis and characterization of an unprecedented 3D lanthanide coordination polymer assembled by cubane-like clusters and a flexible V-shaped dicarboxylate ligand *Inorg. Chem. Commun.* **61** 177
45. Wong H-Y, Chan W T K and Law G-L 2018 Assembly of lanthanide(III) cubanes and dimers with single-molecule magnetism and photoluminescence *Inorg. Chem.* **57** 6893
46. Acharya J, Biswas S, van Leusen J, Kumar P, Kumar V, Narayanan R S, et al. 2018 Exploring tuning of structural and magnetic properties by modification of ancillary β-diketonate co-ligands in a family of near-linear tetranuclear Dy^{III} complexes *Cryst. Growth Des.* **18** 4004
47. Das S, Hossain S, Dey A, Biswas S, Sutter J-P and Chandrasekhar V 2014 Molecular magnets based on homometallic hexanuclear lanthanide(III) complexes *Inorg. Chem.* **53** 5020
48. Biswas S, Das S, Rogez G and Chandrasekhar V 2016 Hydrazone-ligand-based homodinuclear lanthanide complexes: synthesis, structure, and magnetism *Eur. J. Inorg. Chem.* **2016** 3322
49. Biswas S, Das S, Gupta T, Singh S K, Pissas M, Rajaraman G and Chandrasekhar V 2016 Observation of slow relaxation and single-molecule toroidal behavior in a family of butterfly-shaped Ln_4 complexes *Chem. Eur. J.* **22** 18532
50. Biswas S, Das S, Hossain S, Bar A K, Sutter J-P and Chandrasekhar V 2016 Tetranuclear lanthanide(III) complexes containing a square-grid core: synthesis, structure, and magnetism *Eur J. Inorg. Chem.* **2016** 4683
51. Kalita P, Goura J, Manuel Herrera Martínez J, Colacio E and Chandrasekhar V 2019 Homodinuclear LnIII2 (LnIII = GdIII, TbIII, HoIII, and DyIII) complexes: field-induced SMM behavior of the DyIII and TbIII analogues *Eur. J. Inorg. Chem.* **2019** 212
52. Li L-F, Kuang W-W, Li Y-M, Zhu L-L, Xu Y and Yang P-P 2019 A series of new octanuclear Ln_8 clusters: magnetic studies reveal a significant cryogenic magnetocaloric effect and slow magnetic relaxation *New J. Chem.* **43** 1617
53. Li X-L, Wu J, Zhao L, Shi W, Cheng P and Tang J 2017 End-to-end azido-pinned interlocking lanthanide squares *Chem. Commun.* **53** 3026
54. Chen H, Yang X, Jiang D, Shi D and Zhang L 2018 Construction of NIR luminescent polynuclear lanthanide-based nanoclusters with sensing properties towards metal ions *Dalton Trans.* **47** 13880
55. Chandrasekhar V, Bag P and Colacio E 2013 Octanuclear $\{Ln(III)_8\}$(Ln = Gd, Tb, Dy, Ho) macrocyclic complexes in a cyclooctadiene-like conformation: manifestation of slow relaxation of magnetization in the Dy(III) derivative *Inorg. Chem.* **52** 4562
56. Nikolayenko IV, Bazzicalupi C, Thubron G P and Grimmer C 2010 Ethyl (2E)-2-(hydroxyimino)propanoate *Acta Cryst. E* **66** o887
57. Fritsky I O, Kozłowski H, Sadler P J, P. Yefetova O, Świątek-Kozłowska J, Kalibabchuk V A and Głowiak T 1998 Template synthesis of square-planar nickel(II) and copper(III) complexes based on hydrazide ligands *J. Chem. Soc. Dalton Trans.* 3269
58. *SMART & SAINT Software Reference manuals*, version 6.45, Bruker Analytical X-ray Systems, Inc., Madison, WI, 2003
59. *SADABS, Program for Empirical Absorption Correction*, University of Gottingen, Germany, 1996
60. *Bruker APEX2*, version 2008.1−0, Bruker AXS Inc., Madison, Wisconsin, USA, 2008
61. Sheldrick G M 2015 SHELXT-integrated space-group and crystal structure determination *Acta Cryst. A* **71** 3
62. Sheldrick G M 2015 Crystal structure refinement with SHELXL *Acta Cryst. C* **71** 3
63. Dolomanov O V, Bourhis L J, Gildea R J, Howard J A K and Puschmann H 2009 OLEX2: a complete structure solution, refinement and analysis program *J. Appl. Crystallogr.* **42** 339
64. Brown I D 2009 Recent developments in the methods and applications of the bond valence model *Chem. Rev.* **109** 6858
65. Trzesowska A, Kruszynski R and Bartczak T J 2004 New bond-valence parameters for lanthanides *Acta Cryst. B* **60** 174
66. Spek A 2015 PLATON SQUEEZE: a tool for the calculation of the disordered solvent contribution to the calculated structure factors *Acta Cryst. C* **71** 9
67. *DIAMOND*, version 3.2, Crystal Impact GbR, Bonn, Germany, 1997
68. *SHAPE: Continuous Shape Measures calculation*, version 2.1, Electronic Structure Group, Universitat de Barcelona, Spain, 2013.
69. Cirera J, Ruiz E and Alvarez S 2005 Continuous shape measures as a stereochemical tool in organometallic chemistry *Organometallics* **24** 1556
70. Costes J-P, Dupuis A and Laurent J-P 1998 Homodinuclear lanthanide complexes: Ln2L3 (H2L = tetradentate Schiff bases). Magnetic properties (solid state) and spectroscopic studies (solution) *Inorg. Chim. Acta* **268** 125
71. John D and Urland W 2006 Crystal structure and magnetic behaviour of the new gadolinium carboxylates $Gd_2(ClF_2CCOO)_6(hypy)_2$, $Gd_2(F_3CCOO)_6(hypy)_2$,

$Gd_2(F_2HCCOO)_6(hypy)_2$ and $Gd_2(Cl_2HCCOO)_6(H_2O)_2(hypy)_2$ *Eur. J. Inorg. Chem.* **2006** 3503
72. Roy L E and Hughbanks T 2006 Magnetic coupling in dinuclear Gd complexes *J. Am. Chem. Soc.* **128** 568
73. Evangelisti M 2014 In *Molecular Magnets Physics and Applications* J Bartolomé, F Luis and J F Fernández (Eds.) p. 365
74. Bala S, Adhikary A, Bhattacharya S, Bishwas M S, Poddar P and Mondal R 2017 Ln8 (Ln= Gd, Ho, Er, Yb) butterfly core-exhibiting magnetocaloric effect and field-induced SMM behavior for Er analouge *ChemistrySelect* **2** 11341
75. Cui C, Ju W, Luo X, Lin Q, Cao J and Xu Y 2018 A series of lanthanide compounds constructed from Ln_8 rings exhibiting large magnetocaloric effect and interesting luminescence *Inorg. Chem.* **57** 8608
76. Zangana K H, Pineda E M, Schnack J and Winpenny R E P 2013 Octametallic 4f-phosphonate horseshoes *Dalton Trans.* **42** 14045
77. Evangelisti M and Brechin E K 2010 Recipes for enhanced molecular cooling *Dalton Trans.* **39** 4672
78. Sharples J W and Collison D 2013 Reprint of "Coordination compounds and the magnetocaloric effect" *Polyhedron* **66** 15
79. Sessoli R 2012 Chilling with magnetic molecules *Angew. Chem. Int. Ed.* **51** 43
80. Fernando L and Marko E 2015 In *Molecular Nanomagnets and Related Phenomena* S Gao (Ed.) (Berlin Heidelberg: Springer-Verlag) Vol. 164 p. 431
81. Liu J-L, Chen Y-C, Guo F-S and Tong M-L 2014 Recent advances in the design of magnetic molecules for use as cryogenic magnetic coolants *Coord. Chem. Rev.* **281** 26
82. Chen Y-C, Qin L, Meng Z-S, Yang D-F, Wu C, Fu Z, et al. 2014 Study of a magnetic-cooling material $Gd(OH)CO_3$ *J. Mater. Chem. A* **2** 9851
83. Han S-D, Miao X-H, Liu S-J and Bu X-H 2014 Magnetocaloric effect and slow magnetic relaxation in two dense (3,12)-connected lanthanide complexes *Inorg. Chem. Front.* **1** 549
84. Rinehart J D and Long J R 2011 Exploiting single-ion anisotropy in the design of f-element single-molecule magnets *Chem. Sci.* **2** 2078